Agricultural and Forest Meteorology 361 (2025) 110312

Contents lists available at ScienceDirect

Agricultural and Forest Meteorology

journal homepage: www.elsevier.com/locate/agrformet

# High-frequency attenuation in eddy covariance measurements from the LI-7200 IRGA with various heating and filter configurations – a spectral correction approach

Jamie Smidt [a,*], Luise Wanner [b], Andreas Ibrom [c], HaPe Schmid [a], Matthias Mauder [b]

[a] Karlsruhe Institute of Technology, Institute of Meteorology and Climate Research, Atmospheric Environmental Research (IMK-IFU), KIT-Campus Alpin, Kreuzeckbahnstr. 19, 82467 Garmisch-Partenkirchen, Germany
[b] Dept. Environmental Sciences, Technical University of Dresden, Dresden, Germany
[c] Dept. Environmental Engineering, Technical University of Denmark, Lyngby, Denmark

ARTICLE INFO

*Keywords:*
Low-pass filtering
Eddy covariance flux measurements
(en)closed-path IRGA
Spectral correction
ICOS

ABSTRACT

The use of (en)closed-path Infrared Gas Analysers (IRGA) in the measurement of Eddy Covariance (EC) fluxes results in inadvertent high-frequency tube attenuation due to diffusion and mixing of sampled gas inside the tube. The application of tube heating and installation of particulate filters along the tube length also contributes to high-frequency attenuation. The goal of this research is first, to quantify the attenuation effects of different tube heating and filter configurations on $CO_2$ and $H_2O$ fluxes. And second, to present a modified power spectral approach (PSA) based on theoretical power spectra to calculate the effective cut-off frequency *fc*. Measurements for each experimental configuration were performed at an Integrated Carbon Observation System (ICOS) station equipped with the standard LI-7200 enclosed-path IRGA and Gill HS-50 3D sonic anemometer. Correction factors for each dataset were determined and implemented in post-processing. We found only very small attenuation effects of $CO_2$ fluxes between the examined configurations. In agreement with previous studies, we found attenuation worsens with increasing relative humidity *rH*, in the fluxes of $H_2O$. As expected, the highest (best) $f_c$ for $H_2O$ was found in the lowest examined *rH* class of 45-50 % with the configuration of heating on, no filter. The lowest (worst) $f_c$ for $H_2O$ was in the highest *rH* class of 90-95 % with the configuration of heating off with the 7 μm filter. Our results confirm that tube attenuation effects for the standard ICOS setup are negligible for $CO_2$ and small for $H_2O$, depending on tube heating settings and use of particulate filters. We also show that the post-processing of attenuation effects, especially for $H_2O$, could improve the accuracy of long-term EC measurements. We recommend that this novel approach be considered by users of datasets collected with the LI-7200 enclosed-path IRGA.

## 1. Introduction

The eddy covariance (EC) method is the most widely used technique to quantify land-atmosphere exchange of energy, momentum and trace gases (Aubinet et al., 2012; Baldocchi, 2003). Despite significant advancements in instruments and technology over the past decades, the method is inherently imperfect in practice, leaving potential for errors in the flux estimation. This paper addresses frequency response errors, an umbrella term used to describe a number of specific sources of error caused by both low- and high-frequency attenuation in the measurements, and the corrections for those errors. Generally, in the low frequencies, mean-removal by de-trending or block-averaging methods exclude the variance caused by the largest eddies from EC flux estimates, effectively resulting in high-pass filtering (filtering that "passes" the high frequencies, mainly blocking low frequencies). Physical properties of the instruments such as limitations in size, sensor separation distances and sensor response time primarily affect the high frequencies and thus, may introduce implicit low-pass filtering effects (filtering that "passes" the low frequencies, mainly blocking high frequencies). In (en)closed-path Infrared Gas Analyser (IRGA) systems the attenuation of sampled gas in the tube also results in low-pass filtering (Aubinet et al., 2000; Burba, 2013; Ibrom et al., 2007; Massman and Ibrom, 2008). Tube attenuation (also called "dampening" in the literature) is particularly problematic in water vapour flux measurements, usually attributed to

* Corresponding author.
*E-mail address:* jamie.smidt@kit.edu (J. Smidt).

https://doi.org/10.1016/j.agrformet.2024.110312
Received 7 February 2024; Received in revised form 18 September 2024; Accepted 11 November 2024
Available online 20 November 2024

the dipole moment from its molecular structure, which makes $H_2O$ "stickier" and therefore more prone to attenuation along the tube wall than $CO_2$, even if condensation effects are reduced by, e.g., tube heating.

Frequency response errors are virtually invisible in the measured scalar time series. They are most conveniently identified by transforming the time series into the spectral domain (e.g., by a Fast-Fourier-Transform method, FFT). In the spectral domain, the flux is distributed by frequency, rather than time, showing how much of the raw flux is transported at each frequency. Fig. 1 schematically illustrates the effect of low-pass filtering in the spectral signature of an arbitrary scalar, in which the attenuated spectrum drops off from the reference spectrum at the high-frequency end. Following Ibrom et al. (2007), the cut-off frequency $f_c$, is defined as the frequency at which the filter reduces power by a factor of two. The shaded area is proportional to the signal loss due to attenuation.

According to Fratini et al. (2012), low-pass filtering can be the dominant source of error in EC data, depending on relative humidity *rH*. Low-pass filtering always leads to an underestimation of the fluxes (Fig. 1) and can cause significant biases over long periods of time, even contributing to energy balance non-closure.

Signal attenuation in closed-path systems has long been recognized and investigated (Massman and Clement, 2004; Massman, 1991). For comparison purposes, in-situ experiments with co-located closed and open-path sensors have been performed (Ibrom et al., 2007; Runkle et al., 2012). These were used to explore correction methods for the closed-path sensor data, based on the open-path data as reference. Another approach to quantify signal loss from attenuation is the wavelet correction method, which directly corrects for high-frequency losses in EC scalar-flux measurements by adjusting the sampled scalar-concentration time series in the wavelet half-plane, without requiring assumptions about scalar similarity or the shape of the cospectrum (Nordbo and Katul, 2013). Many studies have recognized and quantified the relationship between an increase in relative humidity and an increase in attenuation in closed-path systems (Ammann et al., 2006; Fratini et al., 2012; Ibrom et al., 2007; Massman and Ibrom, 2008; Peltola et al., 2021).

The development of the enclosed path $CO_2/H_2O$ Infrared Gas Analyser (IRGA) (LI-7200; LI-COR Biosciences, Lincoln, NE, USA) aims to optimise the strengths and weaknesses of both the open- and closed-path designs of the past (Burba et al., 2010). The LI-7200, shown schematically in Fig. 2, features an intake tube that can be customized to as short as a few centimeters or as long as several meters, though the recommended length for most EC systems is approximately 0.4 – 1.7 m (Burba et al., 2010; Clement et al., 2009). The LI-7200 was chosen as the standard IRGA for $CO_2$ and $H_2O$ Flux measurements for the initial phase of the European ICOS network (Rebmann et al., 2018). A heated intake tube can also be used to minimize adsorption and desorption of water vapour along the tube wall, which increases signal attenuation (Massman and Ibrom, 2008). Metzger et al. (2016) found that in addition to the properties of the intake tube, the shape of the rain cap and the insect screen at the tube inlet also contributes to the overall attenuation effect. An optional particulate filter can also be installed that causes a (nearly isothermal) pressure drop downstream and leads to the aforementioned benefits of reducing the relative humidity and thus effects from water vapour sorption (e.g., Schmid et al., 2000). When used in environments with airborne dust and pollen, the filter should extend the period of time between cleanings of the optical cell.

The research goal of this paper is twofold. First, we quantify the possible attenuation effects of different heating and filter configurations with the LI-7200 enclosed-path IRGA. Second, we propose a modified power spectral approach (PSA) to calculate the cut-off frequency of these attenuation effects. To our knowledge, no previous research has specifically quantified the attenuation effects of different experimental configurations (heat and filters) of the ICOS standard IRGA and 3D sonic anemometer.

We collected data over time periods of approximately 1-2 weeks per experimental run, using each of six potential heat and filter combinations with the LI-7200: heat on and off, no filter, Swagelok® 2 µm and 7 µm filters. We analysed the power spectra of $CO_2$ and $H_2O$ to identify differences in low-pass filtering effects among each experimental setup, and in the case of $H_2O$, different conditions of relative humidity. We then calculated the cut-off frequency for each dataset, and determined an exponential function for the effects of *rH* on the cut-off frequency of $H_2O$. Using the resulting cut-off frequencies for $CO_2$, and the slope and offset of the exponential function for *rH* and $f_c$ for $H_2O$, we implemented these spectral loss corrections in the eddy covariance flux calculation software TK3 (Mauder and Foken, 2015).

Based on previous research summarized above and recommendations on experimental setup (e.g Metzger et al., 2016), we expected the data with tube heating to show less attenuation than data without tube heating, as the tube heating was specifically designed to decrease water adsorption to the tube walls and therefore deliver a more intact gas mixture over the distance from the intake point of the tube to the measurement chamber of the IRGA. For these reasons, we expected this effect to be particularly obvious in the $H_2O$ measurements. We also expected attenuation of $H_2O$ (and to a lesser degree, $CO_2$) to decrease with decreasing filter size, due to the potentially larger pressure drop across the filter which lowers humidity in the tube; thus measurements using no filter likely show lower cut-off frequencies than datasets with the Swagelok® 7 or 2 µm filters, respectively.

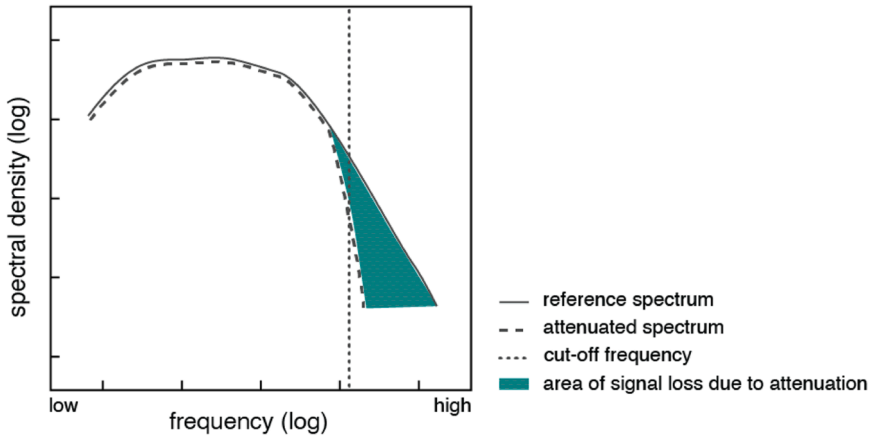


**Fig. 1.** A schematic of a reference spectrum and the attenuated spectral signature of a scalar. Relative to the reference spectrum, the attenuated spectrum is slightly shifted down for display purposes. The deviation of the attenuated spectrum from the reference indicates signal attenuation (dampening) at high frequencies. The cut-off frequency $f_c$, is defined here as the frequency at which the filter reduces power by a factor of two compared to the reference spectrum.

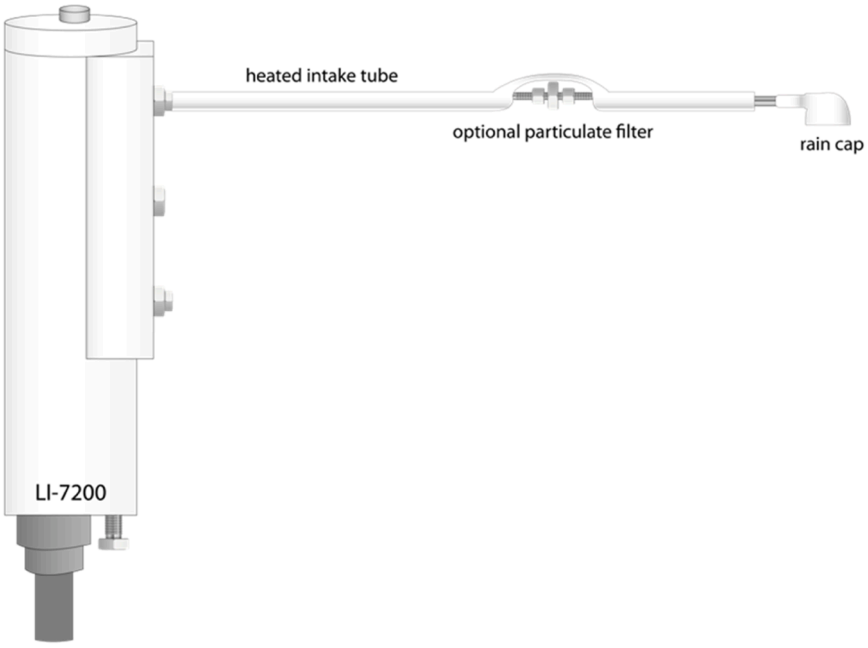


**Fig. 2.** A schematic of the LI-COR Biosciences LI-7200 enclosed path IRGA with heated intake tube including optional particulate filter and rain cap.

## 2. Methods

### 2.1. Site description, instrumentation and data collection

Data was collected at research station Fendt (47.8329°N 11.0607°E; DE-FEN), 595 m asl, located in the southern part of the German state of Bavaria, in a shallow broad valley bottom, set in the foothills of the Alps. The landcover in this area is dominated by grasslands. At Fendt the grassland is intensively managed, with up to six cuts and five manure fertilizer applications per summer (Kiese et al., 2018). Fendt features two fully-equipped EC measurement towers, one that is part of the TERENO-preAlpine observatory (Kiese et al., 2018; Zeeman et al., 2017), and one tower that is part of the Integrated Carbon Observation System (Rebmann et al., 2018). The two towers are approximately 5 m apart. This study examines $CO_2$ and $H_2O$ spectra and flux data measurements from the ICOS tower, which is equipped with a three-dimensional sonic anemometer (model HS-50, Gill Instruments Ltd, Lymington, UK) and an enclosed-path IRGA (LI-7200, LI-COR, Lincoln, NE, USA) with an insulated intake tube (part #7200-050, LI-COR, Lincoln, NE, USA). The combination of these two instruments is the ICOS standard and used at every Class-1 EC station in the network (Rebmann et al., 2018). We grouped the $H_2O$ power spectra into *rH* classes based on measurements from an independent humidity and temperature probe (HMP45, Vaisala, Vaanta, Finland) at a height of 3.5 m, from the Fendt TERENO-preAlpine station.

The Fendt ICOS EC station samples data at a rate of 10 Hz, the core instruments are installed at a height of 3.1 m above ground level, the IRGA firmware version was 8.7.5 (LI-COR, Lincoln, NE, USA, https://www.licor.com/env/support/LI-7200RS/software.html) and throughout the data collection period, the flow rate of the IRGA was steady between approximately 14.5 – 15.5 standard liters per minute. Swagelok® 2 µm (part #SS-4FW-2, Swagelok, Solon, OH, USA) and 7 µm (part #SS-4FW-7) filters can be installed along the length (in our case, 71 cm) of the LI-7200 heated intake tube, with the rain cap version 3 at the tube end. This rain cap version was developed by LI-COR to significantly reduce the low-pass filtering compared to previous, larger versions of the rain cap (Metzger et al., 2016). When in use, tube heat was set at 4 W, the maximum power to be considered effective (Metzger et al., 2016).

Data was collected between late April and late July, 2018. Each possible combination of heat and filter was implemented at the station for approximately 1-2 weeks at a time, not necessarily in sequence, as detailed in Table 1.

### 2.2. Eddy covariance data processing

Proper test of attenuation effects on measured fluxes requires careful raw data post-processing and screening for data quality. The relevant steps and methods are outlined below.

The raw, high-frequency (10 Hz) 3D sonic and scalar data were processed with the "Turbulence Knight 3" (TK3) Eddy Covariance Software package (Mauder and Foken, 2015). TK3 is the newest version of the original package "Turbulenzknecht" developed in 1989 (Foken, 1999) that further evolved into "Turbulence Knight 2" (Mauder et al., 2008). From the raw data, TK3 calculates half-hourly means of the input parameters, in our case $CO_2$ and $H_2O$, their fluxes, variances, covariances, spectra and co-spectra. Data quality assessments are done via a quality flag system, and random errors from instrument noise and the stochastic nature of turbulence (defined as the variance of the covariance, Finkelstein and Sims, 2001) were also calculated, as described in detail by Mauder et al. (2013).

**Table 1**
An overview of the six experimental configurations of heat and filter combinations.

| Code | Heat | Filter | Dates | Number of 30-minute periods available for processing |
|---|---|---|---|---|
| **NHNF** | Off | None | 2018-04-24 to 2018-05-03 and 2018-07-05 to 2018-07-12 | 773 |
| **NH7F** | Off | 7 µm | 2018-07-13 to 2018-07-27 | 653 |
| **NH2F** | Off | 2 µm | 2018-05-22 to 2018-05-29 | 325 |
| **HNF** | On | None | 2018-06-28 to 2018-07-04 | 288 |
| **H7F** | On | 7 µm | 2018-06-14 to 2018-06-20 | 292 |
| **H2F** | On | 2 µm | 2018-06-20 to 2018-06-27 | 336 |

Before 30-minute averaged fluxes were calculated, the raw, high-frequency data underwent several quality control steps. Plausibility tests were performed to exclude physically or electronically impossible values, as defined in Table 1 of Mauder and Foken (2015). A spike detection algorithm based on median absolute deviation analysis was applied to identify and remove outliers (Mauder et al., 2013). And missing data was filled by linear interpolation if at least 90 % of the expected 30-minute data was available (Mauder and Foken, 2015).

The calculation of averages, variances and covariances in each 30-minute timesteps (described in detail in Section 3.2 of Mauder and Foken, 2015) included coordinate rotation to align the coordinate system with the mean wind direction. Lagged covariance analysis was used to account for time lags between variables measured by different instruments (Kaimal and Finnigan, 1994; Mauder et al., 2013; Mauder and Foken, 2015). Spectral corrections were applied to account for low-pass filtering and path averaging effects (Moore, 1986a). Sonic temperature was converted to actual temperature to account for humidity effects (Foken et al., 2012; Schotanus et al., 1983). And covariances, which are generally calculated in kinematic units, were converted to fluxes in energetic units following (Foken, 2008; Stull, 1988a).

Post-processing quality assessments included a steady state test to ensure the net fluxes were representative of the surface flux (Foken and Wichura, 1996; Mauder and Foken, 2015) and an integral turbulence test to verify well-developed turbulence conditions (Foken and Wichura, 1996; Kaimal and Finnigan, 1994; Mauder and Foken, 2015; Stull, 1988). Quality flags from 0 (high) to 2 (low) were assigned based on these tests, following the Spoleto agreement for CarboEurope-IP (Mauder et al., 2013).

In order to investigate the high-frequency spectral loss correction effects of the cut-off frequencies due to tube attenuation, each dataset was initially processed with the aforementioned settings, and then re-processed using the same settings with the single addition of a correction for high-frequency spectral loss from this form of signal attenuation. This correction multiplies the (co)spectrum with a transfer function Eq. (8), defining the signal attenuation after (Moore, 1986) and considers both stable and unstable conditions (Kaimal et al., 1972). We were then able to compare the two datasets before and after spectral correction.

### 2.3. Theoretical basis of the $PSA_{S24}$ method

The first preparatory step in the analysis of filtering effects and calculation of a time constant was the decision to use either a Power Spectral Approach (PSA) or Cospectral Approach (CSA). There is no general consensus in the literature to strongly recommend the use of PSA rather than CSA, or vice versa, in the fluxes of $CO_2$ and $H_2O$. Wintjen et al. (2020) recommends using cospectra for the high-frequency response correction of nitrogen fluxes, and says power spectral methods work well for inert gases. Ibrom et al. (2007) argues in favor of PSA because the vertical wind speed ($w$), which is of course part of the cospectra, does not contribute to the spectral attenuation of the IRGA. The use of CSA also requires careful determination of the time lag due to sensor separation, which distracts from the focus of the present study. Therefore, following Ibrom et al. (2007) and others (Aslan et al., 2020; Fratini et al., 2012; Sabbatini et al., 2018), we elected to use the PSA method.

Our method relies heavily on the results of two of the aforementioned studies (Aslan et al., 2020; Ibrom et al., 2007), both of which used the PSA method to correct for low-pass filtering effects in the measured $CO_2$ and $H_2O$ signals. The $PSA_{I07}$ method developed by Ibrom et al. (2007) performs noise removal and calculation of filtering effects in two separate steps for different frequency ranges, while the $PSA_{A20}$ method by Aslan et al. (2020) processes both in one calculation step using the entire frequency domain.

To perform the power spectral analysis, first the 30-minute power spectra data were combined with other data needed for further processing and filtering, such as mean horizontal wind velocity $u$, the stability parameter $z/L$, absolute humidity and temperature for the calculation of relative humidity, and the variance of $CO_2$ and absolute humidity. Each of these additional variables are derived from the measured data by the TK3 software.

Then, each 30-minute power spectrum was weighted by natural frequency, $f$ and normalized by the corresponding variance of the scalar of interest, as shown in Eq. (1), following (Ibrom et al., 2007):

$$fS_{x,norm} = \frac{S_x \cdot f}{\sigma_x^2} \tag{1}$$

where $S_x$ represents the spectrum of the scalar of interest, $f$ is natural frequency (Hz) and $\sigma_x^2 = \overline{(x')^2}$ is the variance of the scalar of interest.

Next, the spectra were placed into 99 bins of exponentially increasing size, from 0.001 Hz to the Nyquist frequency, which is half the sampling frequency (in our case, data was sampled at 10 Hz, so the Nyquist frequency is 5 Hz). The spectra were then binned by averaging all the spectra in each bin. The number of spectral densities in each bin was also determined. This varies greatly, and was used to weight the data in further processing steps.

$PSA_{A20}$ is a further development of $PSA_{I07}$ introducing a more elegant and effective consideration of the white sensor noise. We primarily follow $PSA_{A20}$ (Aslan et al., 2020). While $PSA_{A20}$ calculates the low-pass filter transfer function using the measured sonic temperature ($T_S$) power spectra as a reference spectrum, we found our $T_s$ spectra to be too noisy (not shown) and inconsistent, with slopes in the inertial subrange deviating strongly from the reference slopes following the Kolmogorov theory (e.g., Kaimal and Finnigan, 1994). This problem resulted in unrealistic, sometimes even negative cut-off frequencies, suggesting that sonic anemometer $T_s$-spectra are not necessarily suitable as reference spectra. This behaviour of the $T_s$-spectra in the inertial subrange is likely related to the well-known problems of the Gill-HS sonic anemometer in measuring temperature fluctuations (see Fig. 4 in Mauder et al., 2006). To avoid dependence on a possibly imperfect measured reference spectrum (e.g., sonic temperature) and to make this experiment independent of other instruments and their errors, a modified approach was developed using a well-proven, universally applicable theoretical spectrum in the inertial subrange (ref), here denoted as $PSA_{S24}$. To achieve the reference inertial subrange slope required by Kolmogorov's Theory, we applied the common expression for spectra and cospectra (e.g., Eq. 4.2 from Massman and Clement, 2004):

$$S_x(f) = A_0 \frac{\frac{f}{f_x}}{\left[1 + m\left(\frac{f}{f_x}\right)^{2\mu}\right]^{\frac{1}{2\mu}\left(\frac{m+1}{m}\right)}} \tag{2}$$

where $S_x$ represents the power spectrum of the scalar of interest (here, $CO_2$ or $H_2O$), $f$ is natural frequency (Hz), $m$ is the inertial subrange slope fixed parameter, $A_0$ is a normalization free parameter, $f_x$ is the spectral peak frequency (Hz) free parameter, and $\mu$ is the broadness free parameter, calculated to approximate the stable and unstable atmospheric cospectra of Kaimal et al. (1972). To describe the spectra, $m = 3/2$ results in a -5/3 power law and was set as a fixed value in the equation. $A_0$, $f_x$, and $\mu$ were determined during the fitting of (2) against the ensemble-averaged, weighted and normalized $CO_2$ or $H_2O$ power spectra. We used starting values of $A_0 = 1$, $f_x = 0.01$, $\mu = 1/4$ (for $CO_2$) and $\mu = ½$ (for $H_2O$). Using a non-linear least-squares Levenberg-Marquardt regression algorithm (nlsLM function from R package minpack.lm, Elzhov et al., 2016), Eq. (2) was fitted to the measured (weighted and normalized, see Eq. (1)) power spectrum of the scalar of interest. Because random noise becomes dominant in the high-frequency end, the equation fitting was limited to power spectral frequencies of less than 1 Hz. In the $PSA_{A20}$ method, Aslan et al. (2020) used the measured and normalized temperature spectrum as the

reference (their Eq. 7):

$$fS_{x,norm}(\mathrm{PSA_{A20}}) = f\frac{S_T(f)}{\sigma_T^2}F_{norm}\frac{1}{1+(2\pi f\tau)^2}+fb, \tag{3}$$

where $f$ is natural frequency (Hz), $F_{norm}$ is a normalization free parameter, $\tau$ is the time constant and $b$ is the y-axis intercept of the power spectrum of white noise. $F_{norm}$, $\tau$ and $b$ are determined from the fitting of Eq. (3) to the measured spectrum of the scalar of interest and the reference spectrum.

However, as explained above, the $\mathrm{PSA_{S24}}$ method uses the theoretical relation Eq. (2) as its reference spectrum, instead of the sonic temperature power spectra $\frac{S_T(f)}{\sigma_T^2}$:

$$fS_{x,ref}(\mathrm{PSA_{S24}}) = \left(\frac{\frac{f}{f_x}}{A_0\left[1+m\left(\frac{f}{f_x}\right)^{2\mu}\right]^{\frac{1}{2\mu}\left(\frac{m+1}{m}\right)}}\right)F_{norm}\frac{1}{1+(2\pi f\tau)^2}+fb, \tag{4}$$

where $x$ needs to be replaced by $CO_2$ or $H_2O$, as the case may be. We used starting values of $F_{norm} = 1.2$, $\tau = 0.18$ and $b = -4$ in the fitting algorithm. The output parameters of Eq. (4) are therefore $F_{norm}$, $\tau$ and $b$. To convert $\tau$, the time constant, to the cut-off frequency $f_c$, we used the following from Moore (1986):

$$f_c = \frac{1}{2*\pi*\tau}. \tag{5}$$

In both cases, i.e. for $CO_2$ and $H_2O$, Eq. (4) was used as regression model to determine $f_c$. For $CO_2$, the entire dataset of each experimental configuration was used. However, for $H_2O$, the data of each configuration was binned in relative humidity *rH* classes of 5 % width covering the observed range of *rH* and the regression model was fitted for each *rH* class individually. The results were one cut-off frequency for each $CO_2$ configuration and 9 cut-off frequency estimates (corresponding to the 9 *rH* classes) for each $H_2O$ configuration.[1]

The $H_2O$ spectra were binned into *rH* classes based on measurements from an independent humidity and temperature probe (HMP45, Vaisala, Vaanta, Finland). Because the spectra are sorted into 99 exponential bins, a single 30-minute observation has 99 spectral data points. To be included in the analysis, we required that each *rH* class must have had a minimum of 6 30-minute valid observations, which corresponds to a spectral sample size of $N = 594$. As previously mentioned, the $\mathrm{PSA_{S24}}$ method presented here was applied to each *rH* class to find $f_c$. Following (e.g., Fig. 2 from Fratini et al., 2012), we plotted *rH* against $f_c$ for each dataset to fit an exponential curve, chosen due to the shape suggested by the data points. The resulting coefficients of the exponential curve then became the correction factor for each $H_2O$ configuration. Those coefficients, and the cut-off frequencies for $CO_2$, were used to determine the signal attenuation for each experimental setup. Using a spectral transfer function derived from Moore (1986), each dataset was reprocessed, and the power spectra multiplied by Eq. (6) for $CO_2$ and Eq. (7) for $H_2O$:

For $CO_2$, the spectral transfer function is

$$T_{CO_2}(f)_{corrected} = \frac{1}{\left[1+\left(\frac{f}{f_c}\right)^4\right]}fS_{CO_2,ref}(\mathrm{PSA_{S24}}) \tag{6}$$

where $f$ is natural frequency (Hz), and $f_c$ is the cut-off frequency. And for $H_2O$, the spectral transfer funtion is

$$T_{H_2O}(f)_{corrected} = \frac{1}{\left[1+\left(e^{m\,\cdot\,rH+\,b}\right)^4\right]}fS_{H_2O,ref}(\mathrm{PSA_{S24}}), \tag{7}$$

where $m$ is the slope and $b$ is the y-intercept of the exponential relationship of *rH* and $f_c$. Again following Moore (1986), the transfer functions from Eq. (6) and Eq. (7) was then implemented across all frequencies to calculate $\frac{\Delta F}{F}$, the error of a flux from spectral loss:

$$\frac{\Delta F}{F} = 1-\frac{\int_0^\infty T_x(f)_{corr}\cdot fSco_{xy,ref}df}{\int_0^\infty fSco_{xy,ref}df}, \tag{8}$$

where $T_x(f)_{corr}$ is the product of the transfer functions describing the spectral response of wind velocities, and $CO_2$ Eq. (6) or $H_2O$ Eq. (7), and $fSco_{xy,ref}$ is the theoretical form of the cospectrum between $wCO_2$ and $wH_2O$.

## 3. Results

The resulting cut-off frequencies of each experimental configuration for $CO_2$ are shown in Fig. 3. The lowest cut-off frequency (corresponding to the most signal attenuation) was found in the experimental configuration of H7F with $f_c = 2.1 \pm 0.21$ Hz (Fig. 3d). The configuration of HNF showed the highest cut-off frequency (corresponding to the least signal attenuation) with $f_c = 4.2 \pm 1.03$ Hz (Fig. 3b).

The $H_2O$ spectra in Fig. 4 were processed using the same method as $CO_2$, but the data was first split into *rH* classes of 5 %. The x-axis lower limit of Fig. 4 was set to $10^{-2}$ Hz in order to show the high frequencies in more detail, as tube attenuation has the strongest effect in that area of the spectrum. The cut-off frequencies $f_c$ and sample sizes (representing the number of 30-minute EC observations) are shown in each panel of the plot. We found, as humidity increases, the scatter of the measured ensemble spectra also increases, and the peak region of the curve shifts to the right (to lower frequencies). In humidity classes of 90 % and above, the peak region effectively disappears, and the curve shows only the inertial subrange. Also, the temperature and humidity probe we used for *rH* measurements is slightly less reliable at high humidities, perhaps due to hysteresis of *rH* at and near saturation levels. Kyrouac and Theisen (2017) found the uncertainty of the HMP45 to be ±2 % between 0 and 90 % *rH* and ±3 % above 90 % *rH*. For these reasons, we excluded *rH* classes of 90-95 % and 95-100 % from our analysis.

For the most part, the $f_c$ decreases with increasing *rH*. The highest cut-off frequency (i.e., the least amount of attenuation) was found in the HNF configuration, with $f_c = 3.09 \pm 1.43$ Hz in the lowest *rH* class, 45-50 %. The lowest cut-off frequency (i.e. the highest amount of attenuation) $f_c = 0.08 \pm 0$ Hz was found in the highest *rH* class, 85-90 %, in the NH7F configuration.

The largest sample sizes were generally found in the highest *rH* classes, with the smallest sample sizes in the lowest and mid-range *rH* classes. The largest sample size was in the NHNF configuration, which also had the most available data points in total, at 80-85 % *rH* with $N = 80$. The smallest sample size was $N = 7$ in the NH7F configuration at 70-75 % *rH*.

Using the relative humidity *rH* classes and the resulting cut-off frequencies $f_c$ of each experimental configuration as determined in Fig. 4, an exponential relationship was determined by a linear least-square

[1] The method by Aslan et al. (2021) Eq. (3) applies a linear transformation of the power spectrum by multiplying it with the frequency to better characterize the white noise. Multiplication with the frequency is a standardized way of representing turbulence spectra in micro-meteorology (see, e.g. Stull, 1988). As one of our reviewers mentioned, it might be confusing that the dependent variable ($fS_x$) is an arithmetic function of the independent variable ($f$) , which might be seen as compromising the theory of regression. However, this error-free linear transformation of both of the empirical data and the reference spectrum does not affect the information relevant for the determination for $f_c$, which lies solely in the difference between the empirical $S_x$ and the theoretical one (Eq. 4). Aslan et al. (2021), found that the fitting was more robust this way compared to alternatives.

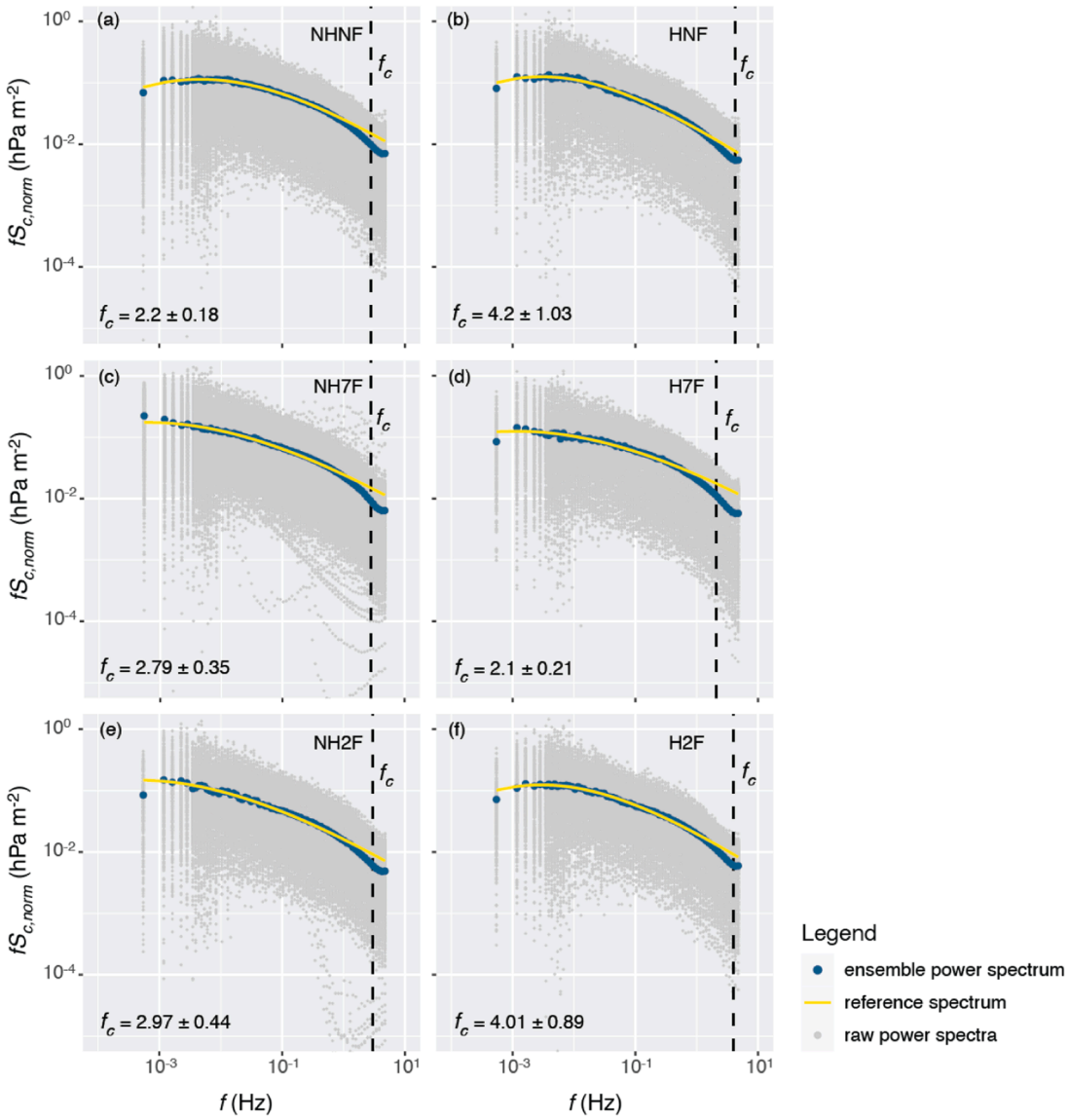


**Fig. 3.** The reference spectrum, calculated with the Massman and Clement (2004) general mathematical expression of spectra (yellow line), plotted with the ensemble power spectrum of $CO_2$ (blue dots), modeled with the reference spectrum against natural frequency. The $CO_2$ cut-off frequency (see Eq. (4) and Eq. (5)), is shown with the error of the individual regressions as indicators of uncertainty. Refer to Table 1 for the configuration codes.

regression method. The data and regression curves are plotted together in Fig. 5.

In general, the fitted function was close to the data, with coefficients of determination ($r^2$) values between 0.89 and 0.97. The NHNF configuration shows the highest offset of 4.7. The lowest regression offset (*b*) of 3 was found in the NH2F configuration.

To illustrate the correction effects of this method, in Fig. 6 we plotted the mean of corrected and uncorrected latent heat fluxes against the difference between the corrected and uncorrected latent heat fluxes for each experimental configuration, versus color-coded *rH* class (on the left) and *z/L* (on the right) As expected, there was no discernible correction effects in the fluxes of sensible heat and $CO_2$, so those results are not shown. Examination of the distribution (also not shown) of the differences between the corrected and uncorrected latent heat flux values showed in the vast majority of cases, a correction was not necessary. The largest differences between the corrected and uncorrected latent heat fluxes were in the cases where, at most, a relatively coarse filter was applied (NHNF and NH7F). Fig. 6 also shows that there is a considerable dependence of the correction on *rH*, as expected, but a dependence on *z/L* is weak or not apparent.

## 4. Discussion and conclusions

The first research goal of this paper is to quantify the attenuation effects of different heating and filter configurations at the Fendt ICOS station. The Fendt ICOS station was built according to ICOS standards outlined by Rebmann et al. (2018) and the installation and customization of the IRGA closely follows the suggestions of Metzger et al. (2016). Therefore, our IRGA was already optimized to minimize frequency response errors and overall, our cut-off frequencies reflect these improvements.

We found no evidence that the cut-off frequencies for $CO_2$ respond to different heat and filter configurations. We could not attribute the comparatively low cut-off frequency for the dataset of heating on, 7 μm filter (Fig. 3) to any particular factor, however the low sample size may contribute. In the case of $CO_2$, instrumental setup may only have a negligible effect on tube attenuation and specifically optimizing heat and filter configurations for the $CO_2$ flux may not be a primary concern. Other decision-making factors regarding the $CO_2$ instrumentation will probably be more important, such as the fact that smaller filters have to be cleaned and changed more often, and that tube heating requires a

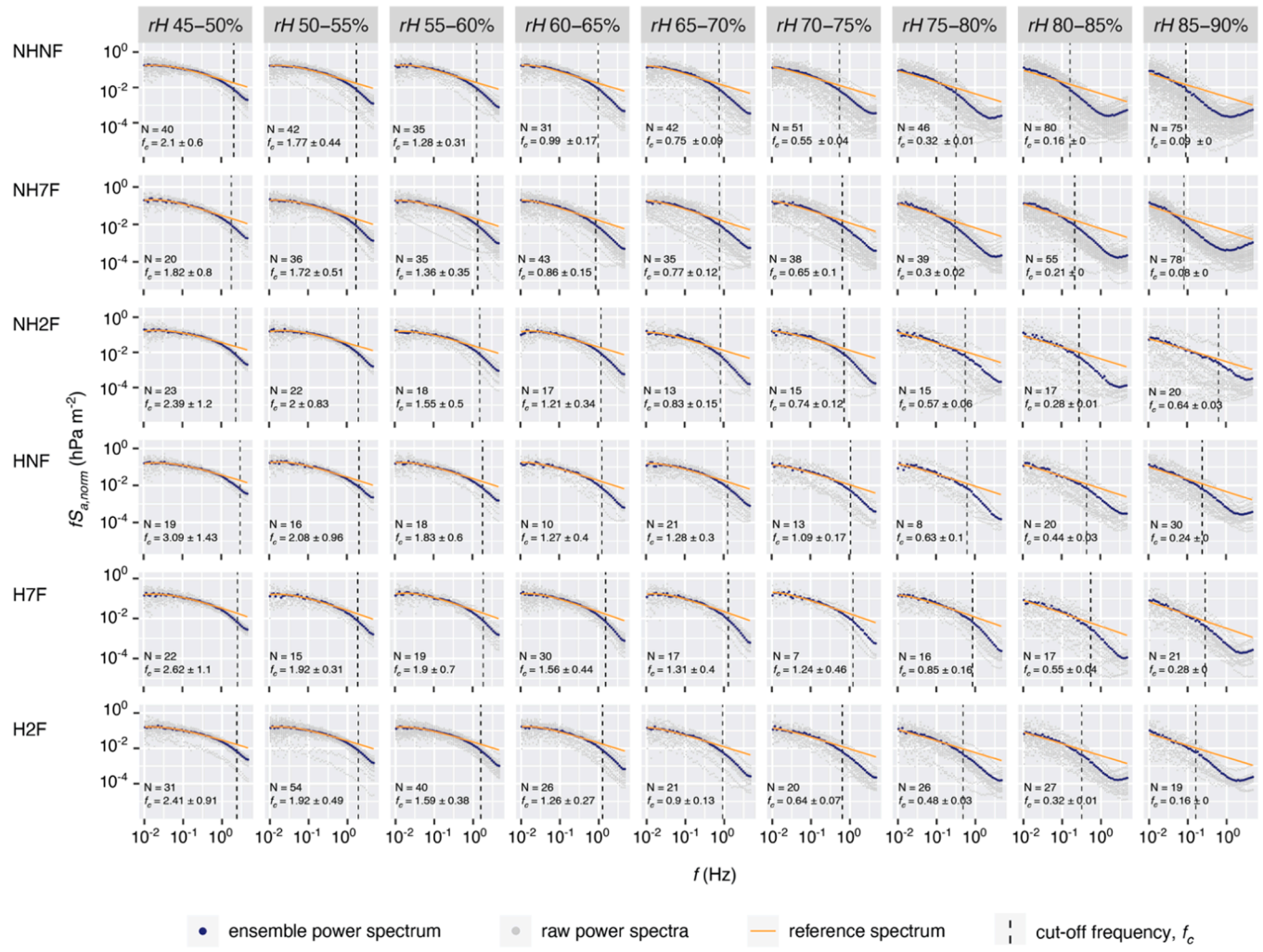


**Fig. 4.** Composite plot of $H_2O$ spectral analysis showing the effect of *rH* on $f_c$ for each experimental configuration. The orange line is the reference spectrum, calculated with the Massman and Clement (2004) general mathematical expression of spectra. The blue dots are the ensemble power spectrum of $H_2O$, modeled with the reference spectrum. The raw power spectra data is shown in grey dots. The black vertical dashed line indicates the cut-off frequency $f_c$, for each experimental configuration and *rH* class. The cut-off frequency (calculated with Eq. (4) and Eq. (5)), is shown with the error of the individual regressions as indicators of uncertainty. Due to high uncertainty at and near *rH* saturation levels, we exclude *rH* classes above 90 % from this analysis. The lower limit of the x-axis has been set to $10^{-2}$ to better focus on the high-frequency end of the plots, where attenuation occurs.

reliable power supply, etc.

We found tube attenuation worsens with increasing relative humidity for $H_2O$, in agreement with a number of previous studies (Ammann et al., 2006; Fratini et al., 2012; Ibrom et al., 2007; Massman and Ibrom, 2008; Peltola et al., 2021), with slightly better cut-off frequencies in datasets with tube heating on (Fig. 4). The highest (lowest attenuation) $f_c$ of 3.09 ± 1.43 Hz was found in the dataset of heating on, no filter at the lowest *rH* class of 45-50 %. The lowest (highest attenuation) $f_c$ of 0.08 ± 0 Hz was found in the dataset of heating off, 7 μm filter at the *rH* class of 85-90 %. Compared to Fratini et al. (2012), which performed a similar analysis with the LI-7200 (without tube heating or filters), our cut-off frequencies were much higher. Fratini et al. (2012) showed that in conditions of low *rH* (defined as 30 %) low-pass filtering occurred at 0.44 Hz, and for high *rH* (defined as 70 %) the signal dropped at 0.13 Hz. For the configuration of heat off, no filter (our most similar setup to Fratini et al., 2012), our results show $f_c = 2.1 \pm 0.6$ Hz at 45-50 % *rH* (the lowest *rH* class for which sufficient data was available), $f_c = 0.75 \pm 0.09$ Hz at 65-70 % *rH* and $f_c = 0.55 \pm 0.04$ Hz at 70-75 % *rH*. These differences are probably due in part to the fact that the LI-7200 used by Fratini et al. (2012) was an early model not yet optimized based on the work of Metzger et al. (2016), especially with respect to the rain cap.

Neither the $CO_2$ nor the $H_2O$ data showed consistently higher cut-off frequencies with filters installed, as initially expected. It is likely the reduced humidity effects of the pressure drop across the filter is more apparent in systems with longer intake tubes or other factors in our experimental setup negated the effect.

The second research goal of this work is to present a modified method to calculate the cut-off frequency of high-frequency attenuation in order to apply a spectral correction to the measurements. Due to high-frequency noise in the Gill-HS sonic anemometer spectra, we found this $PSA_{S24}$ approach, which uses a general mathematical expression (Massman and Clement, 2004) as reference spectrum in the calculation of Eq. (3) (Aslan et al., 2020) to be more robust than using the measured sonic temperature spectrum itself. Since the Gill HS Sonic Anemometer and LI-7200 are the standard instruments for ICOS observatories, we propose this new method to be an option for the post processing of ICOS data and EC setups where similar attenuation effects were found.

In the analysis of the correction effects of this method on the latent heat flux (Fig. 6), the greatest differences in the correction magnitudes occurred in the configurations without tube heating and at instances of high relative humidity and stable atmospheric conditions, which are of

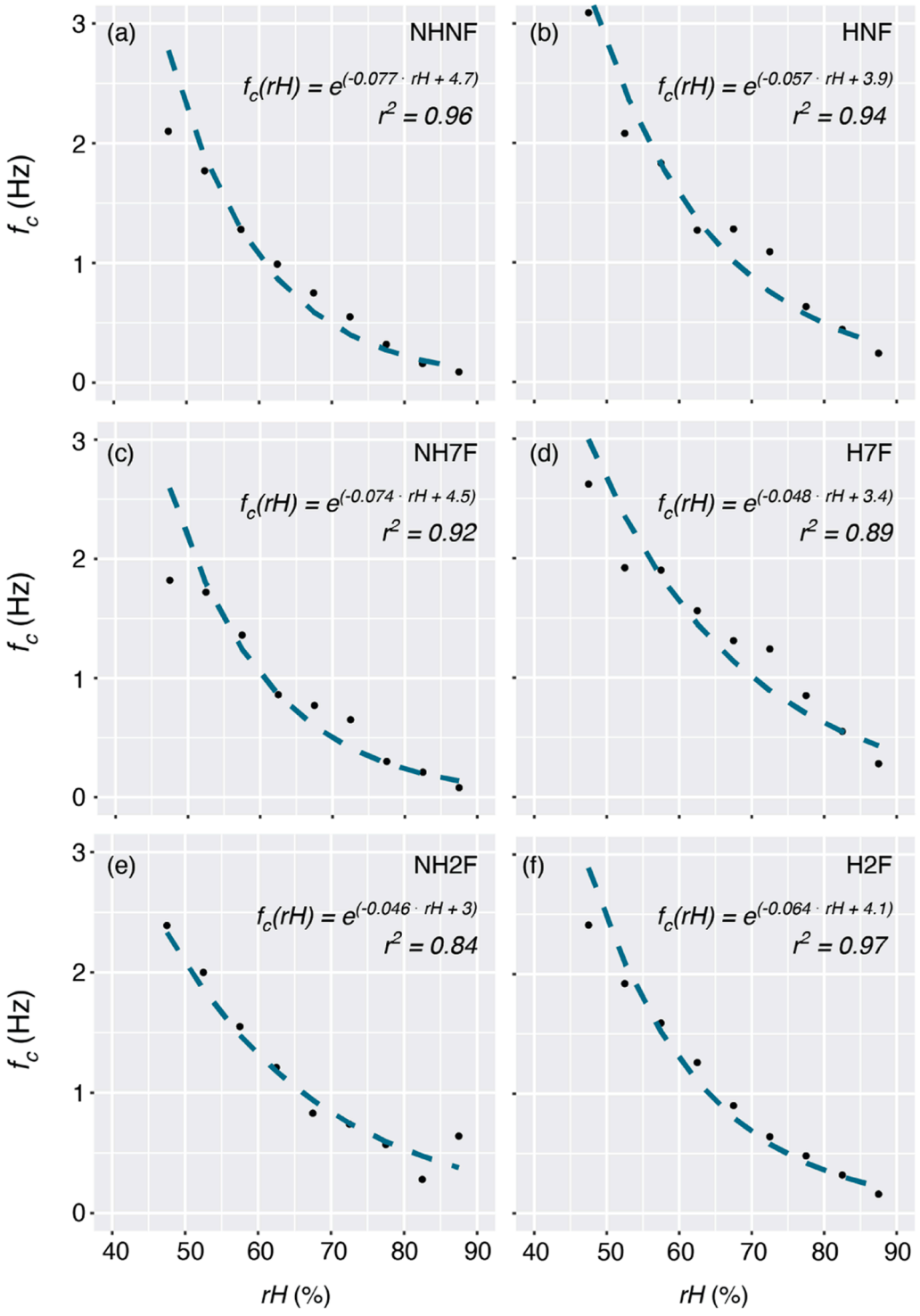


**Fig. 5.** The cut-off frequency is plotted against *rH* for each experimental configuration (black dots). An exponential curve was fitted to the data (blue line), using a linear least-square regression method. The exponential function and $r^2$ of $f_c$ and *rH* are shown for each experimental configuration as determined in Fig. 4.

course somewhat correlated. The two datasets without tube heating also had the largest sample sizes, corresponding to the longest measurement periods and potentially more varied weather conditions, which may contribute to these results. These correction factors are specific to our site and the weather conditions during data collection and are not transferable to other sites.

Overall, our results show that high-frequency attenuation in $CO_2$ fluxes at the Fendt ICOS EC station is negligible. The cut-off frequencies of $H_2O$ worsened with increasing relative humidity, but showed improvement with the use of tube heating. Tube heating of the LI-7200 enclosed IRGA, as recommended by Metzger et al. (2016) is important and should be considered for all ICOS sites. The error percentages (not shown) of the datasets without tube heating ranged from 13 to 17 %, while the datasets with tube heating had between 3 and 6 % error. We show the ICOS standard LI-7200 enclosed-path IRGA at Fendt to be quite robust in terms of low high-frequency attenuation with six combinations of heating and particulate filter use.

Again, it should be noted that the results presented here are specific

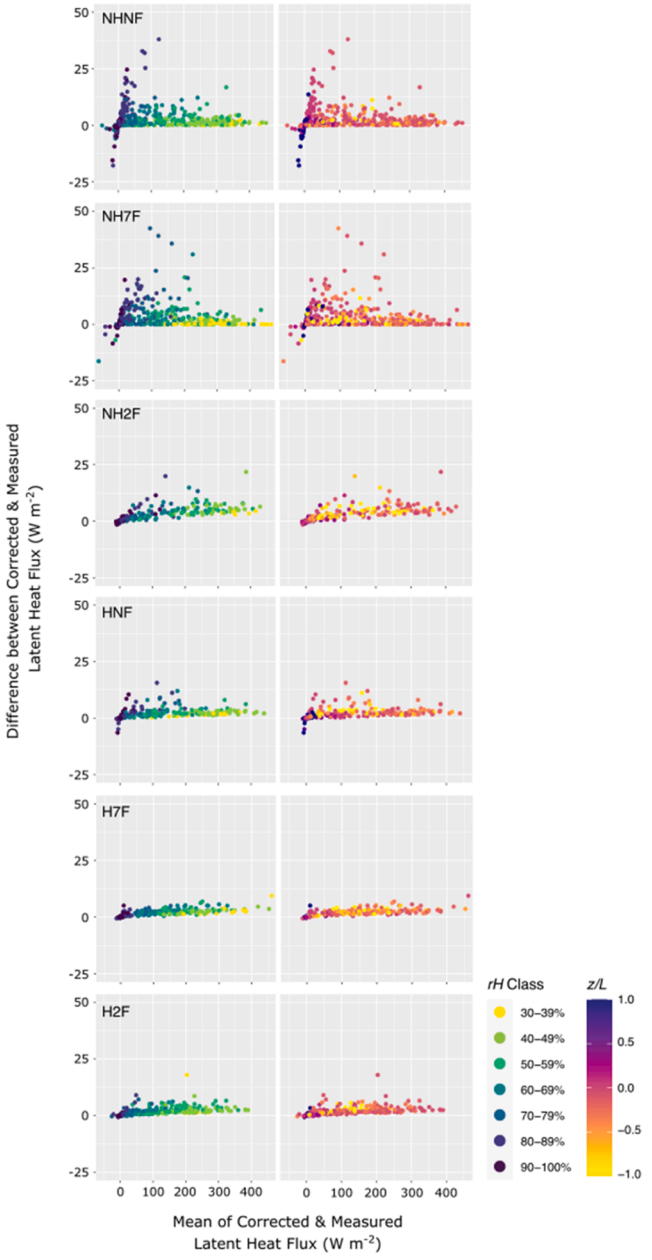


**Fig. 6.** Using the slope and offset of the exponential functions in Fig. 5 as correction factors, the $H_2O$ data was reprocessed and the corrected latent heat flux is plotted against the original latent heat flux for each experimental configuration. In the left column, the data are shown in terms of relative humidity *rH* and in the right column, in terms of the stability parameter *z/L*. The magnitude of the correction Eq. (8) is plotted here, rather than the relative error, for display purposes in cases of small flux values.

to our site, experimental setup, and weather conditions during data collection. As we have yet to develop a general correction to be applied across research sites and EC station configurations, the exponential correction functions must be determined empirically. To best minimize frequency response errors in EC systems, a thoughtful experimental design, specific to measurement site and research goals, with the latest instrument manufacturer recommendations regarding configuration and accessories, is necessary. Post processing can then be used to correct some of the remaining low-pass filtering. We recommend that high-frequency attenuation and spectral analysis be performed for all ICOS sites, according to tube heating and filter size, to determine if, and to what degree, data correction is necessary. For most research purposes and measurement campaigns at ICOS sites using the standard instrumentation, the correction of high-frequency attenuation could be unnecessary. For investigation or presentation of long-term measurements, spectral correction may improve the accuracy of EC measurements from ICOS stations.

## CRediT authorship contribution statement

**Jamie Smidt:** Writing – original draft, Visualization, Software, Methodology, Investigation, Formal analysis, Conceptualization. **Luise Wanner:** Writing – review & editing, Software, Methodology. **Andreas Ibrom:** Writing – review & editing, Methodology. **HaPe Schmid:** Writing – review & editing, Supervision, Funding acquisition. **Matthias Mauder:** Writing – review & editing, Supervision, Methodology, Conceptualization.

## Declaration of competing interest

The authors declare that they have no known competing financial interests or personal relationships that could have appeared to influence the work reported in this paper.

## Acknowledgements

We thank Dr. Ingo Völksch and Dr. Janina Klatt for technical support and maintenance at the Fendt EC stations. Research at the TERENO-preAlpine observatory is funded by the German Helmholtz Association, through its programs ATMO and *Changing Earth*, and the German Federal Ministry of Education and Research (BMBF). ICOS RI is jointly funded by national funding agencies from all ICOS partner countries. More information can be found at www.icos-cp.eu. JS benefitted from participation in the Helmholz Graduate Research Programme Mechanisms & Interactions of Climate Change in Mountain Regions (MICMOR) at KIT-Campus Alpine.

## Data availability

The authors do not have permission to share data.

## References

Ammann, C., Brunner, A., Spirig, C., Neftel, A., 2006. Technical note: water vapour concentration and flux measurements with PTR-MS. Atmos. Chem. Phys. 6 (12), 4643–4651. https://doi.org/10.5194/acp-6-4643-2006.

Aslan, T., Peltola, O., Ibrom, A., Nemitz, E., Rannik, Ü., Mammarella, I., Rannik, U., Mammarella, I., 2020. The high-frequency response correction of eddy covariance fluxes - Part 2: an experimental approach for analysing noisy measurements of small fluxes. *Atmospheric Measurement Techniques, submitted* (7), 5089–5106. https://doi.org/10.5194/amt-14-5089-2021.

Aubinet, M., Grelle, A., Ibrom, A., Rannik, Ü., Moncrieff, J., Bernhofer, C., Clement, R., Elbers, J.A., Granier, A., Grünwald, T., Morgenstern, K., Pilegaard, K., Rebmann, C., Snijders, R., Valentini, R., Vesala, T., 2000. Estimates of the annual net carbon and water exchange of forests: the EUROFLUX methodology. Adv. Ecol. Res. 30, 113–175. https://doi.org/10.1016/S0065-2504(08)60047-1.

Aubinet, M., Vesala, T., Papale, D., 2012. Eddy covariance: a practical guide to measurement and data analysis. Eddy Covariance. Springer, Dordrecht, the Netherlands. https://doi.org/10.1007/978-94-007-2351-1.

Baldocchi, D.D., 2003. Assessing the eddy covariance technique for evaluating carbon dioxide exchange rates of ecosystems: Past, present and future. Glob. Chang. Biol. 9 (4), 479–492.

Burba, G.G., 2013. Eddy Covariance Method for Scientific, Industrial, Agricultural and Regulatory Applications, A Field Book of Measuring Ecosystem Gas Exchange and Areal Emission Rates. LI-COR Biosciences, Lincoln, Nebraska.

Burba, G.G., Mcdermitt, D.K., Anderson, D.J., Furtaw, M.D., Eckles, R.D., 2010. Novel design of an enclosed CO2/H2O gas analyser for eddy covariance flux measurements. Tellus, Series B: Chem. Phys. Meteorol. 62 (5), 743–748. https://doi.org/10.1111/j.1600-0889.2010.00468.x.

Clement, R.J., Burba, G.G., Grelle, A., Anderson, D.J., Moncrieff, J.B., 2009. Improved trace gas flux estimation through IRGA sampling optimization. Agric. For. Meteorol. 149 (3–4), 623–638. https://doi.org/10.1016/j.agrformet.2008.10.008.

Elzhov, T.V., Mullen, K.M., Spiess, A.-N., Bolker, B., 2016. minpack.lm: R Interface to the Levenberg-Marquardt Nonlinear Least-Squares Algorithm Found in MINPACK. Plus Support for Bounds. R package version 1. *2-1*.

Finkelstein, P.L., Sims, P.F., 2001. Sampling error in eddy correlation flux measurements. J. Geophys. Res. Atmospheres 106 (D4). https://doi.org/10.1029/2000JD900731.
Foken, T., 1999. Der Bayreuther Turbulenzknecht 1 (1), 19.
Foken, T., 2008. Micrometeorology. Springer.
Foken, T., Leuning, R., Oncley, S.P., Mauder, M., Aubinet, M, 2012. Corrections and data quality. In: Aubinet, M., Vesala, T., Papale, D. (Eds.), Eddy Covariance: A Practical Guide to Measurement and Data Analysis. Springer, Dordrecht, Heidelberg, London, New York, pp. 85–131.
Foken, T., Wichura, B., 1996. Tools for quality assessment of surface-based flux measurements. Agric. For. Meteorol. 78 (1–2), 83–105. https://doi.org/10.1016/0168-1923(95)02248-1.
Fratini, G., Ibrom, A., Arriga, N., Burba, G., Papale, D., 2012. Relative humidity effects on water vapour fluxes measured with closed-path eddy-covariance systems with short sampling lines. Agric. For. Meteorol. 165, 53–63. https://doi.org/10.1016/j.agrformet.2012.05.018.
Ibrom, A., Dellwik, E., Flyvbjerg, H., Jensen, N.O., Pilegaard, K., 2007. Strong low-pass filtering effects on water vapour flux measurements with closed-path eddy correlation systems. Agric. For. Meteorol. 147 (3–4), 140–156. https://doi.org/10.1016/j.agrformet.2007.07.007.
Kaimal, J.C., Finnigan, J.J., 1994. Atmospheric boundary layer flows: their structure and measurement. Oxford Univ. Press. Oxford University Press, New York. https://doi.org/10.1017/CBO9781107415324.004.
Kaimal, J., Wyngaard, J., Izumi, Y., Cote, O., 1972. Spectral characteristics of surface-layer turbulence. Quarterly J. Royal Meteorolog. Society 098 (417), 563–589. https://doi.org/10.1256/smsqj.41706.
Kiese, R., Fersch, B., Baessler, C., Brosy, C., Butterbach-Bahl, K., Chwala, C., Dannenmann, M., Fu, J., Gasche, R., Grote, R., Jahn, C., Klatt, J., Kunstmann, H., Mauder, M., Rödiger, T., Smiatek, G., Soltani, M., Steinbrecher, R., Völksch, I., Schmid, H.P., 2018. The TERENO pre-alpine observatory: integrating meteorological, hydrological, and biogeochemical measurements and modeling. Vadose Zone J. 17 (1), 180060. https://doi.org/10.2136/vzj2018.03.0060.
Kyrouac, J., & Theisen, A. (2017). Biases of the MET Temperature and Relative Humidity Sensor (HMP45) Report. United States: N. p., 2017. Web. https://doi.org/10.2172/1366737.
Massman, W., Clement, R., 2004. Uncertainty in eddy covariance flux estimates resulting from spectral attenuation. Handbook of Micrometeorology, pp. 67–99. https://doi.org/10.1007/1-4020-2265-4_4.
Massman, W.J., 1991. The attenuation of concentration fluctuations in turbulent flow through a tube. J. Geophys. Res. 96 (D8), 15, 269-15,273.
Massman, W.J., Ibrom, A., 2008. Attenuation of concentration fluctuations of water vapor and other trace gases in turbulent tube flow. Atmos. Chem. Phys. 8, 9819–9853. https://doi.org/10.5194/acp-8-6245-2008.
Mauder, M., Cuntz, M., Drüe, C., Graf, A., Rebmann, C., Schmid, H.P., Schmidt, M., Steinbrecher, R., 2013. A strategy for quality and uncertainty assessment of long-term eddy-covariance measurements. Agric. For. Meteorol. 169, 122–135. https://doi.org/10.1016/j.agrformet.2012.09.006.
Mauder, M., Foken, T., 2015. Documentation and Instruction Manual of the Eddy-Covariance Software Package TK3 (update). Arbeitsergebnisse, UniversitätBayreuth, Abt. Micometeorologie, Bayreuth.
Mauder, M., Foken, T., Clement, R., Elbers, J.A., Eugster, W., Grünwald, T., Heusinkveld, B., Kolle, O., 2008. Quality control of CarboEurope flux data - Part 2: Inter-comparison of eddy-covariance software. Biogeosciences. 5 (2), 451–462. https://doi.org/10.5194/bg-5-451-2008.
Mauder, M., Oncley, S.P., Vogt, R., Weidinger, T., Ribeiro, L., Bernhofer, C., Foken, T., Kohsiek, W., Bruin, H.a.R., Liu, H., 2006. The energy balance experiment EBEX-2000. Part II: Intercomparison of eddy-covariance sensors and post-field data processing methods. Boundary. Layer. Meteorol. 123 (1), 29–54. https://doi.org/10.1007/s10546-006-9139-4.
Metzger, S., Burba, G., Burns, S.P., Blanken, P.D., Li, J., Luo, H., Zulueta, R.C., 2016. Optimization of an enclosed gas analyzer sampling system for measuring eddy covariance fluxes of H2O and CO2. Atmos. Meas. Tech. 9 (3), 1341–1359. https://doi.org/10.5194/amt-9-1341-2016.
Moore, C.J., 1986. Frequency response corrections for eddy correlation systems. Boundary. Layer. Meteorol. 37 (1–2), 17–35. https://doi.org/10.1007/BF00122754.
Nordbo, A., Katul, G., 2013. A Wavelet-Based Correction Method for Eddy-Covariance High-Frequency Losses in Scalar Concentration Measurements. Boundary. Layer. Meteorol. 146 (1), 81–102. https://doi.org/10.1007/s10546-012-9759-9.
Peltola, O., Aslan, T., Ibrom, A., Nemitz, E., Rannik, Ü., Mammarella, I., 2021. The high frequency response correction of eddy covariance fluxes. Part 2: the empirical approach and its interdependence with the time-lag estimation. Atmospheric Measurement Techniques Discussions January, 1–27. https://doi.org/10.5194/amt-2020-479.
Rebmann, C., Aubinet, M., Schmid, H., Arriga, N., Aurela, M., Burba, G., Clement, R., De Ligne, A., Fratini, G., Gielen, B., Grace, J., Graf, A., Gross, P., Haapanala, S., Herbst, M., Hörtnagl, L., Ibrom, A., Joly, L., Kljun, N., Franz, D., 2018. ICOS eddy covariance flux-station site setup: a review. Int. Agrophys. 32 (4). https://doi.org/10.1515/intag-2017-0044.
Runkle, B.R.K., Wille, C., Gažovič, M., Kutzbach, L., 2012. Attenuation correction procedures for water vapour fluxes from closed-path eddy-covariance systems. Boundary. Layer. Meteorol. 142 (3), 401–423. https://doi.org/10.1007/s10546-011-9689-y.
Sabbatini, S., Mammarella, I., Arriga, N., Fratini, G., Graf, A., Hörtnagl, L., Ibrom, A., Longdoz, B., Mauder, M., Merbold, L., Metzger, S., Montagnani, L., Pitacco, A., Rebmann, C., Sedlák, P., Šigut, L., Vitale, D., Papale, D., 2018. Eddy covariance raw data processing for CO 2 and energy fluxes calculation at ICOS ecosystem stations. Int. Agrophys. 32 (4), 495–515. https://doi.org/10.1515/intag-2017-0043.
Schmid, H.P., Grimmond, C.S.B., Cropley, F., Offerle, B., Su, H.B., 2000. Measurements of CO2 and energy fluxes over a mixed hardwood forest in the mid-western United States. Agric. For. Meteorol. 103 (4), 357–374. https://doi.org/10.1016/S0168-1923(00)00140-4.
Schotanus, P., Nieuwstadt, F.T.M., De Bruin, H.A.R., 1983. Temperature measurement with a sonic anemometer and its application to heat and moisture fluxes. Boundary. Layer. Meteorol. 26 (1), 81–93.
Stull, R.B., 1988. An Introduction to Boundary Layer Meteorology. Springer.
Wintjen, P., Ammann, C., Schrader, F., Brümmer, C., 2020. Correcting high-frequency losses of reactive nitrogen flux measurements. Atmos. Meas. Tech. 13 (6), 2923–2948. https://doi.org/10.5194/amt-13-2923-2020.
Zeeman, M.J., Mauder, M., Steinbrecher, R., Heidbach, K., Eckart, E., Schmid, H.P., 2017. Reduced snow cover affects productivity of upland temperate grasslands. Agric. For. Meteorol. 232, 514–526. https://doi.org/10.1016/j.agrformet.2016.09.002.